Electronic Supplementary Material (ESI) for Journal of Materials Chemistry A.

Supplementary Information

Experimental section

In this study, WO_3 NHs were prepared using oblique angle deposition (OAD). In the subsequent step, flame vapor deposition (FVD) as a convenient and universal post-treatment method was used to deposit WO_3 NNs on the as-prepared NHs in a reducing atmosphere. During this process, substoichiometric tungsten oxide was grown on the partially reduced surface of the NHs. After re-annealing in air, a WO_3 photoanode with NNs epitaxial growth on NHs was obtained.

*Fabrication of the WO_3 NHs***.**

WO_3 NHs were fabricated by the OAD method. This method was used for fabricating the NHs due to its time-efficient deposition rate and accurate shape-controlling ability, which is well suited for fabricating specific nanostructures with precise geometries. First, a fluorine-doped tin oxide (FTO, TEC-8, Pilkington) conductive substrate (2 cm×1 cm) was prepared and placed in an e-beam evaporation chamber with tungsten oxide powder (WO_3, Taewon Scientific Co.). Second, the substrate was spun for 2 s at 1 rpm and then stopped for 12 s with an 80° oblique angle and a 3.5 Å s^{-1} deposition rate for the helix array fabrication. The entire process was conducted in the chamber under a pressure of 1.5×10^{-6} Torr. Finally, the as-deposited samples were annealed at 500°C for 2 h.

*Fabrication of the WO_3 NNs***.**

The WO_3 NNs on the surface of the NHs were synthesized using the flame vapor deposition (FVD) method,[1-3] which was done by first growing the crystalline substoichiometric $W_{18}O_{49}$ samples under fuel-rich conditions (a CH_4 to air flow ratio of 18.4 SLPM:12.5 SLPM) on the as-prepared NHs for 5 min, 10 min, and 20 min. The FVD process was realized by oxidizing the tungsten metal into sub-stoichiometric tungsten oxide in the reducing atmosphere, and turning the tungsten oxide into vapor phase using flame under 1000°C. The tungsten oxide vapor condensed on top of cooling surface of the substrate (550°C in this work) and started to grow there. By controlling the synthesis parameters including the fuel/air ratio, the substrate temperature, along with the vapor source concentration, the 1D structure of tungsten oxide was controlled as following the previous works.[1-3] During which the surfaces of the WO_3 NHs were reduced simultaneously. The as-fabricated WO_3 NN/NH was further annealed in air at 500°C for 1 h. In this way, the crystalline NNs were deposited on both top and side of the NH arrays. Using the FVD method, the amount of grown NNs were precisely controlled by tuning the deposition time.

Fabrication of heterojunction system.

In the final part of this study, Mo doped $BiVO_4$ (Mo:$BiVO_4$) was added to the WO_3 NN/NH to testify its role as a host material. To prepare the Mo:$BiVO_4$ precursor solution, 100 mM bismuth(III) nitrate pentahydrate ($BiN_3O_9{\cdot}6H_2O$, Aldrich), 96 mM vanadyl acetylacetonate ($C_{10}H_{14}O_5V$, Aldrich), and 570 μM ammonium heptamolybdate ($(NH_4)_6Mo_7O_{24}{\cdot}4H_2O$, Aldrich) were dissolved in a solvent mixture of 4.46 ml of acetylacetone ($C_5H_8O_2$, Aldrich) and 0.54 ml of acetic acid (CH_3COOH, Aldrich). The Mo:$BiVO_4$ precursor was dispensed onto the as-prepared WO_3 NN/NH host layer twelve times. After each dispensing step, the sample was then allowed to dry at room temperature and annealed at 200°C and 400°C for 5 min and 500°C for 10 min on top of a hot plate. The final annealing process was conducted at 500°C for 2 h. The as-prepared samples were immersed in a 0.5 M potassium hydroxide solution for ten seconds, followed by rinsing in DI water and a drying process, which is used for two-electron pathway measurement. In addition, the Fe-NiOOH OEC layer was deposited by the following procedures to facilitate water oxidation through four-electron pathway. First, in a 0.1 M iron(II) sulfate heptahydrate ($FeSO_4{\cdot}7H_2O$, Aldrich) solution, the FeOOH layer was deposited under 0.25 V *vs.* Ag/AgCl for 17 min, and then, in a 0.1 M nickel(II) sulfate hexahydrate ($NiSO_4{\cdot}6H_2O$, Aldrich) solution, the NiOOH layer was deposited under 0.11 V *vs.* Ag/AgCl for 8 min. Both of the procedures were conducted under light illumination. In the next step, the as-prepared samples were further deposited under 1.2 V *vs.* Ag/AgCl for 1.5 min in the nickel precursor without light illumination.

PEC performance measurements and other characterization steps

Electrolyte

For $WO_{3,}$ the electrolyte used in this study was a 1 M H_2SO_4 solution to minimize the loss via chemical dissolution in the neutral electrolyte. The test marked as "checked in hole scavenger electrolyte" was carried out in 0.5M K_2SO_3 buffered to pH 7. For the four-electron pathway measurement, phosphate buffer solution was used for evaluating the WO/BVO/OEC while for the two-electron pathway case, 2M $KHCO_3$ was used for evaluating WO/BVO.

Measurement system

Both four-electron and two-electron pathway used the three-electrode system to give a better control on the water oxidation reaction, in which the photoanode was used as the working electrode with Ag/AgCl as the reference electrode and Pt foil as the counter electrode. For the two-electron pathway, the measurement was done in the reactor with membrane in between to separate the working and counter compartments. The bottom half of the reactor is immersed in ice water and CO_2 gas was used to keep purging the electrolyte.

Other aspects related to the PEC measurement

To create the metal contacts for the photoanode, silver paste was attached to the top of the anode-exposed area. The irradiance spectrum of the light source was measured and shown in Figure S13. The IPCE was checked with the help of a monochromator (Polaronix K3100 IPCE Measurement System, McScience).

Characterizations

The experimental data for the optical properties were measured using a UV-Vis spectrophotometer (UV-2401 PC, Shimadzu). XRD measurements were carried out using a Siemens diffractometer D500/5000 in the Bragg-Brentano geometry. Morphology analyses of the samples were carried out using a field-emission scanning electron microscope (JSM-7000F, Japan) and a JEOL JEM-2100F (Japan) transmission electron microscope. O_2 evolution from four-electron pathway was detected by the Gas chromatography (GC) measurement. The instant detection of H_2O_2 from two-electron pathway was done using the standard H_2O_2 strips (Indigo Instruments), while the final accumulated amount was further confirmed with a titration process using potassium permanganate ($KMnO_4$, ⩾99.0%, Aldrich), with sulfuric acid (H_2SO_4, Acros Organics) as the H^+ source, based on that the dark purple color of permanganate ion disappears during titration when the MnO_4^- is totally consumed:

$$2MnO_4^- + 5H_2O_2 + 6H^+ \rightarrow 2Mn^{2+} + 5O_2 + 8H_2O$$

The FE for H_2O_2 and O_2 production (%) in this work is defined as

$$FE = \frac{detected\ amount\ \ (mol)}{theoretical\ maximum} \times 100$$

Where the theoretical maximum amounts of H_2O_2 and O_2 are equal to the total number of electrons divided by two and four (in mol), respectively.

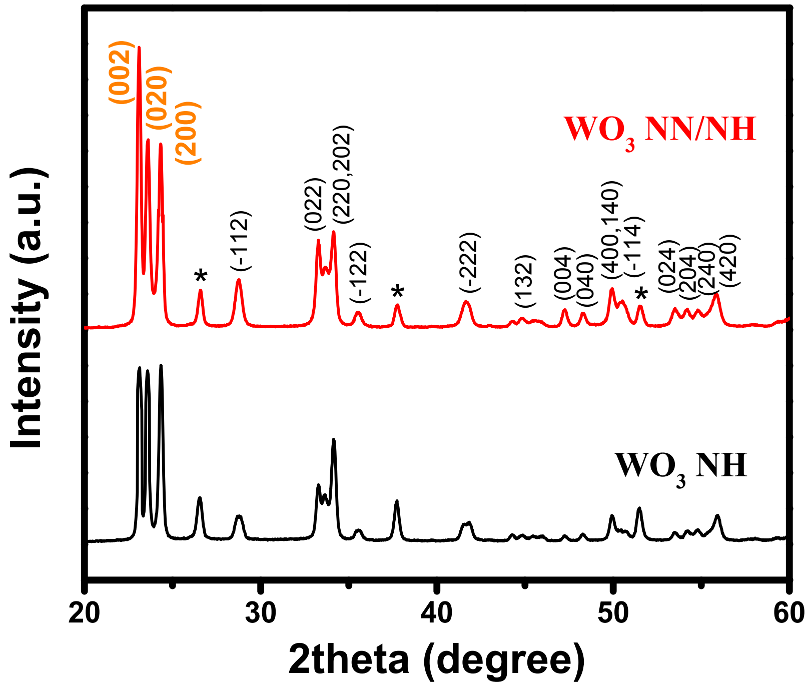

Figure S1. XRD spectra for the NH (black) and the NN/NH (red) showing crystallinity of the NHs and NN/NH. The asterisks (*) indicate the peaks for FTO. The NN/NH has high ratios of (002) to (020) and (200), which is 1.54:1.03:1; while the intensities of these three planes in the NHs are similar, with a ratio 0.99:0.97:1.

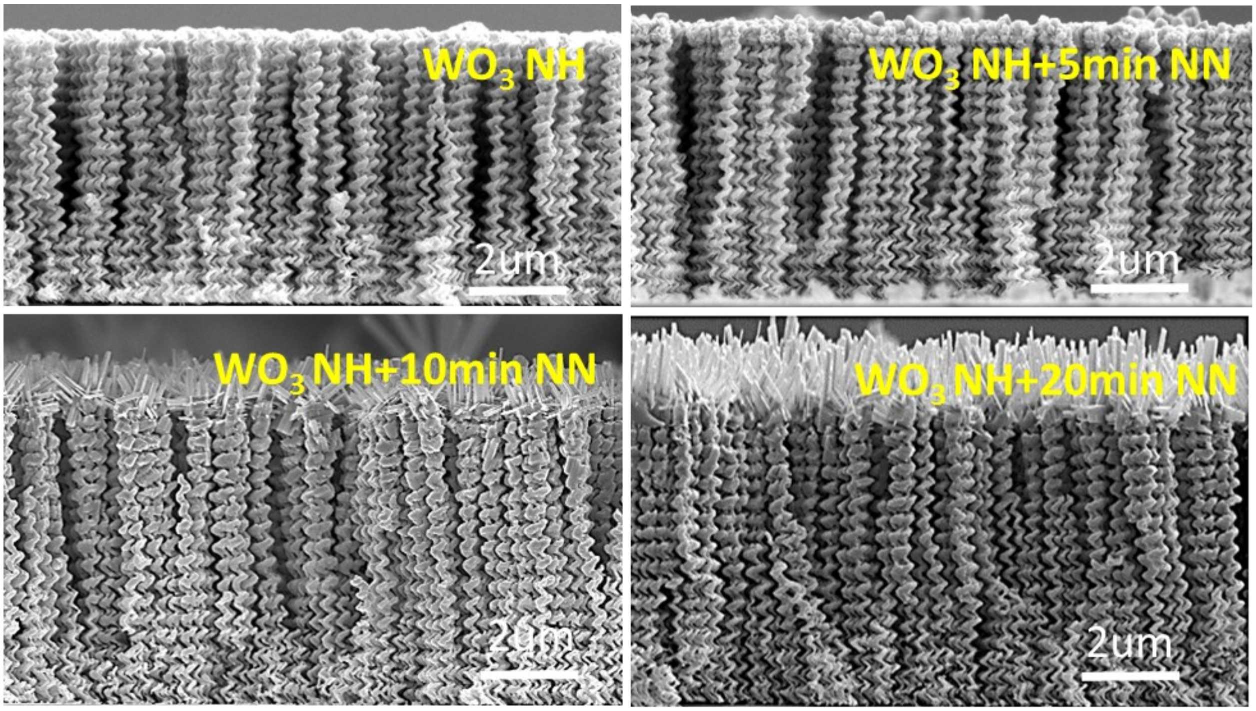

Figure S2. The optimization process of flame growth of WO_3 NNs on WO_3 NHs is shown from this figure to Figure S4. Three varieties of FVD times for the post-growth process to grow WO_3 NNs were applied, *i.e.* 5 min, 10 min and 20 min. The 20 min one has the best performance, and "WO_3 NN/NH" in the main text only represents the 20 min sample. Longer post-regrowth times than 20 min leads to an increase in both the operation time and precursor amount, as well as a decline in current density, which lowers the performance to cost ratio and, therefore, is not adopted in this study. The figures here show the section views of the WO_3 NHs, and WO_3 NHs after 5 min, 10 min, and 20 min flame growth of WO_3 NNs (corresponding to the 5 min, 10 min, and 20 min NN marked in the images). The length of the top NNs increases gradually with the increasing FVD time, and the NNs on the top are longer than the NNs on the side, especially for the 20 min one, which forms a carrot-shaped structure.

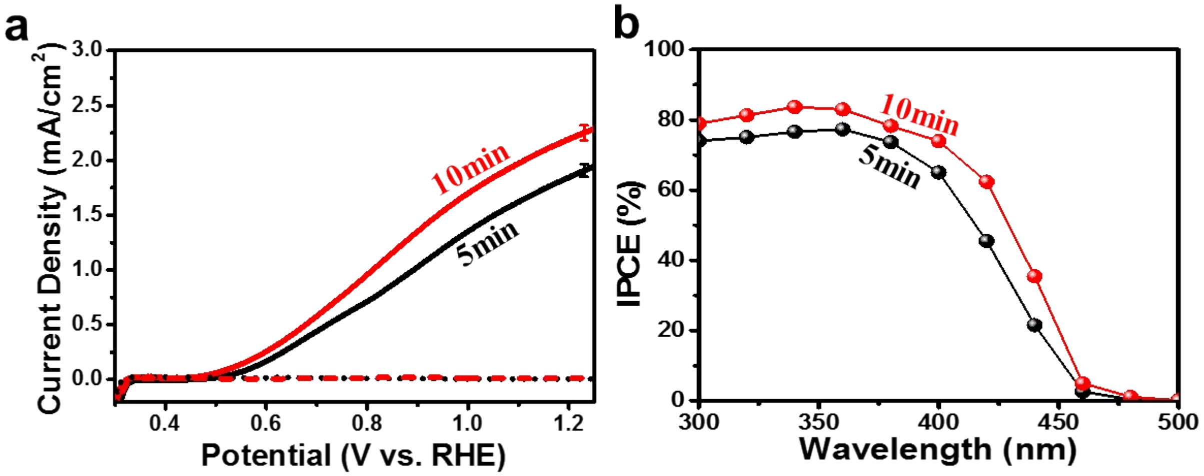

Figure S3. (a) The photocurrent density in terms of the external bias (*J-V*) and (b) the IPCE curves for the NHs after 5 min (black) and 10 min (red) flame growth of NNs (note that the "NN/NH" shown in the main text represents the NHs after 20 min flame growth of NNs, as mentioned in the caption of Figure S2). The error bars show the standard deviation of current densities at 1.23V vs. RHE. The dashed lines are the corresponding dark curves for each measurement. These figures here are presented as supplementary information to Figure 3 to show the evolution of the PEC performance as the post-regrowth time increases.

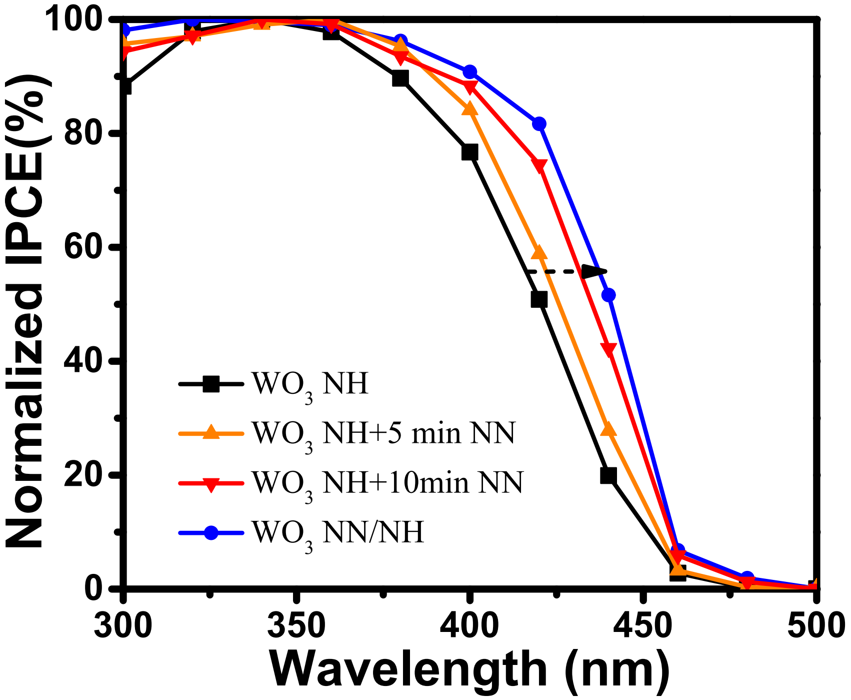

Figure S4. Normalized IPCE of the NHs (black) and the ones after 5 min (blue), 10 min (orange), and 20 min (NN/NH, red) post-growth of NNs. The IPCE used here before normalization are obtained from Figure 3b and Figure S3b. From this figure the enhanced light absorption of NN/NH compared to NH can be detected.

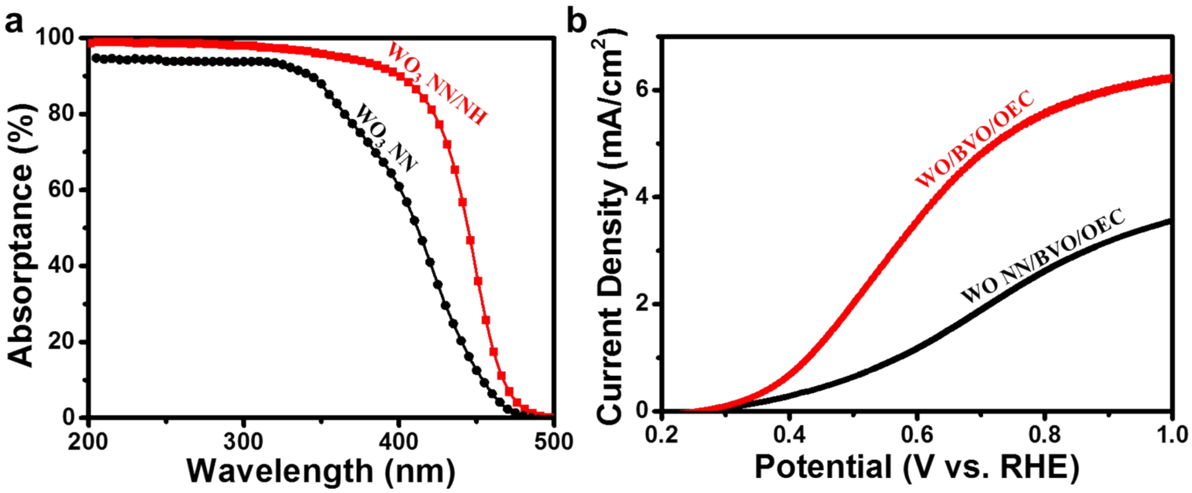

Figure S5. The comparison between WO_3 NN/NH and pure WO_3 NNs of (a) the light absorption. As an indirect bandgap material with a low-magnitude absorption coefficient, WO_3 needs a dense sample with sufficient thickness to fully absorb the photons, especially the ones with lower energies right above the band edge. It can be seen that with NHs as the structure foundation, the NN/NH shows great advantage over NN on light absorption especially for the wavelength near the band edge. (b) the *J-V* curve shows WO_3(NN/NH)/Mo:$BiVO_4$/Fe-NiOOH (WO/BVO/OEC) and WO_3 NN/Mo:$BiVO_4$/Fe-NiOOH (WO NN/BVO/OEC) in a phosphate buffer. Since in the main text mainly the significance of NN coating is shown compared to pure NHs, this supplementary result helps show the function of NH, which could be ascribed to its favorable light absorption ability, the more contact area for $BiVO_4$, and the synergetic effect for hole transport from the VB band position difference between NHs and NNs.

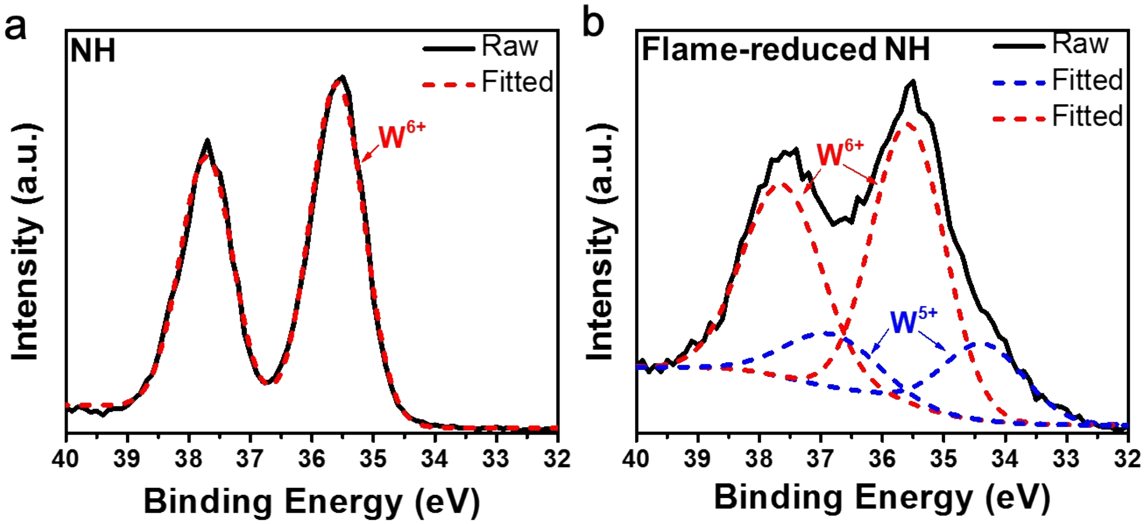

Figure S6. XPS spectra of (a) the WO_3 NHs and (b) the as-reduced NHs before re-annealing. The spectra after flame-reduction treatment in (b) show unambiguous W^{5+} characteristics caused by the oxygen substoichiometry, while the NHs only have peaks of W^{6+}. Solid and dashed lines are measured and fitted data. Some O_2 vacancy could remain after annealing.

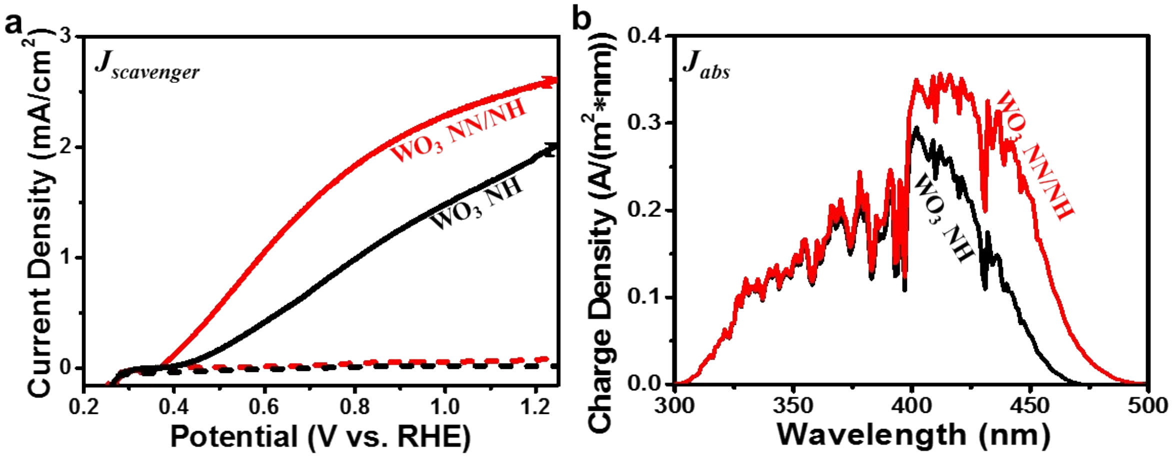

Figure S7. (a) *J-V* curves of the WO_3 NH (black) and the WO_3 NN/NH (red) measured in the hole scavenger electrolyte ($J_{scavenger}$). (b) Charge density obtained from the photon flux by multiplying the light absorptance by the charge of one electron (1.6×10^{-19} C). The theoretical maximum current densities after considering light absorption (J_{abs}) for the WO_3 NH and the WO_3 NN/NH were obtained by integrating their two charge density curves which were used for the charge transport and transfer efficiency calculations in Figure 4c and d.

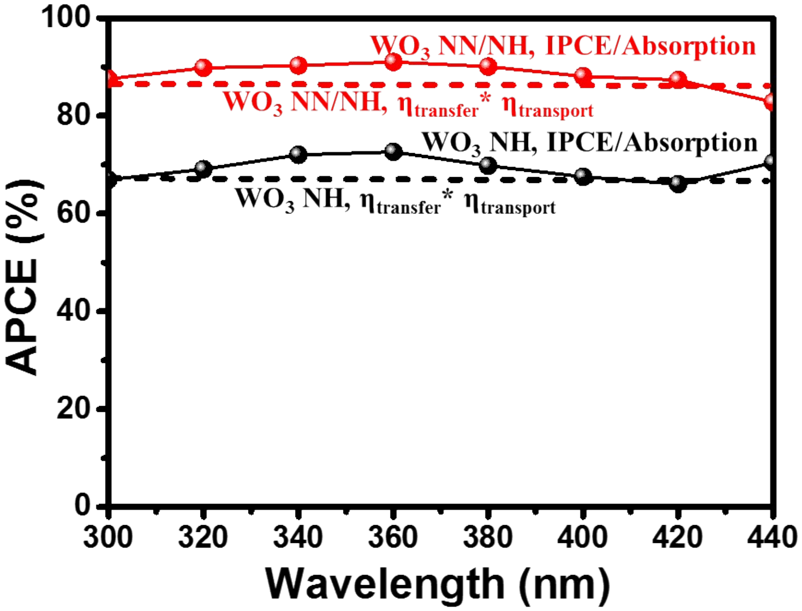

Figure S8. APCE curves for the WO_3 NH (black) and the WO_3 NN/NH (red) which are obtained from two routes: IPCE/Absorptance (solid line, where "/" means "divided by") and $\eta_{transport}$* $\eta_{transfer}$ (dashed line). Both IPCE and $\eta_{transport}\times\eta_{transfer}$ here use the data at 1.23 V *vs.* RHE. Both solid lines agree well with their dashed lines. In addition, the APCE of the NN/NH is higher than the NH in a broad wavelength range, which implies the advantage of the NN/NH on the charge transport and transfer efficiencies over the NH.

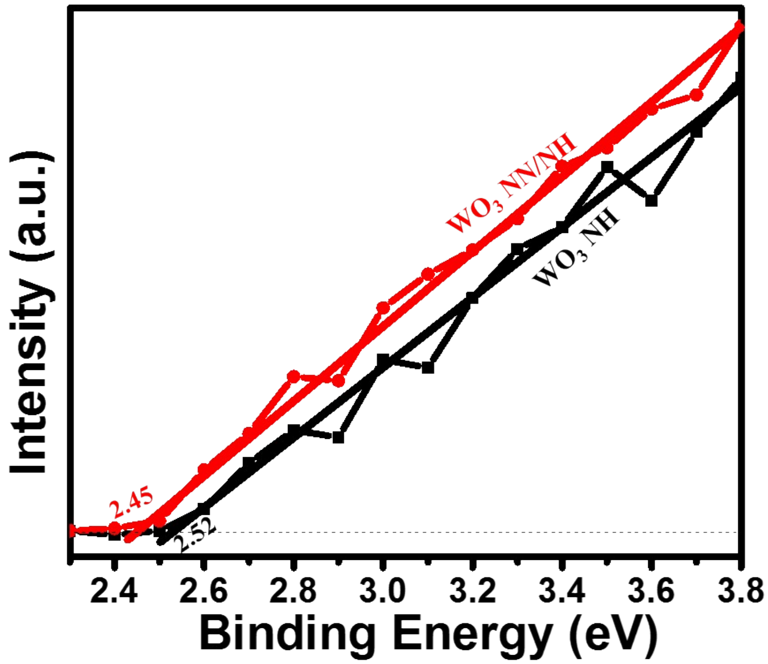

Figure S9. VB maximum measurements from XPS VB spectra for the WO_3 NH (black) and the WO_3 NN/NH (red) in which the NN/NH shows an elevated band edge for VB relative to the NH due to the addition of surface NNs. Such VB position difference between NHs and NNs is beneficial for driving the hole transport, from the bottom NHs to the surface NNs for water oxidation.

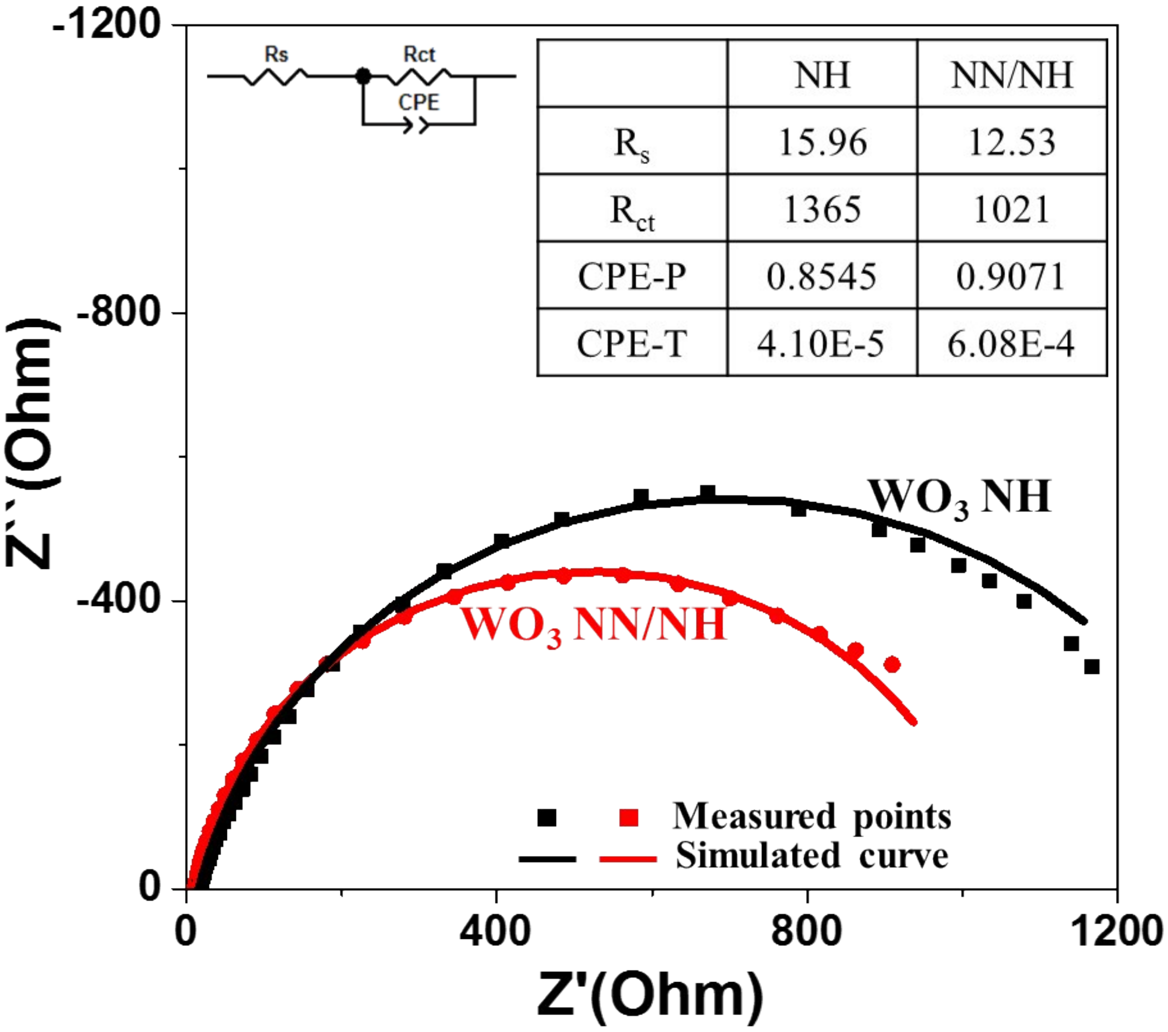

	NH	NN/NH
R_s	15.96	12.53
R_{ct}	1365	1021
CPE-P	0.8545	0.9071
CPE-T	4.10E-5	6.08E-4

Figure S10. Nyquist plots of WO_3 NH (black) and WO_3 NN/NH (red) under 1.23 V *vs.* RHE. The values of the simulated components are shown in Table S1. Sinceresistance from the external system, such as the electrolyte, electrical series, and FTO substrate, among other components, was constant for both NH and NN/NH, the slightly lower Rs value of NN/NH indicates the less bulk resistance of the sample. In addition, the overall smaller value of Rct (charge transfer resistance) and the larger value of CPE (constant phase element) indicated a more efficient charge transfer process crossing the electrode-electrolyte interface after NNs coating.

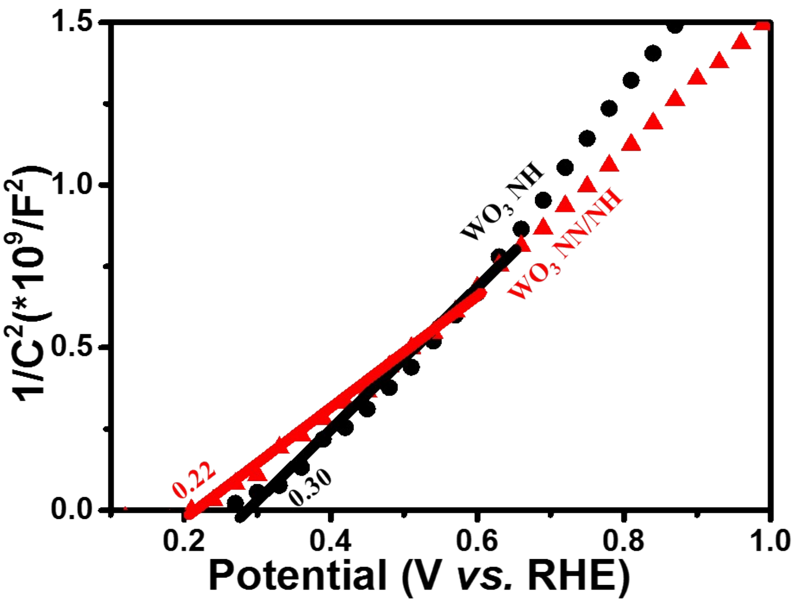

Figure S11. Mott-Schottky plots of the WO_3 NH (black) and the WO_3 NN/NH (red). The intercepts of the tangent lines on the x-axis correspond to their flat band potentials V_{fb}, which are indications of their theoretical photocurrent onset, and the slopes of the tangent lines correspond to their charge carrier densities (N_d), which could be influenced by the effectiveness of the charge separation process.

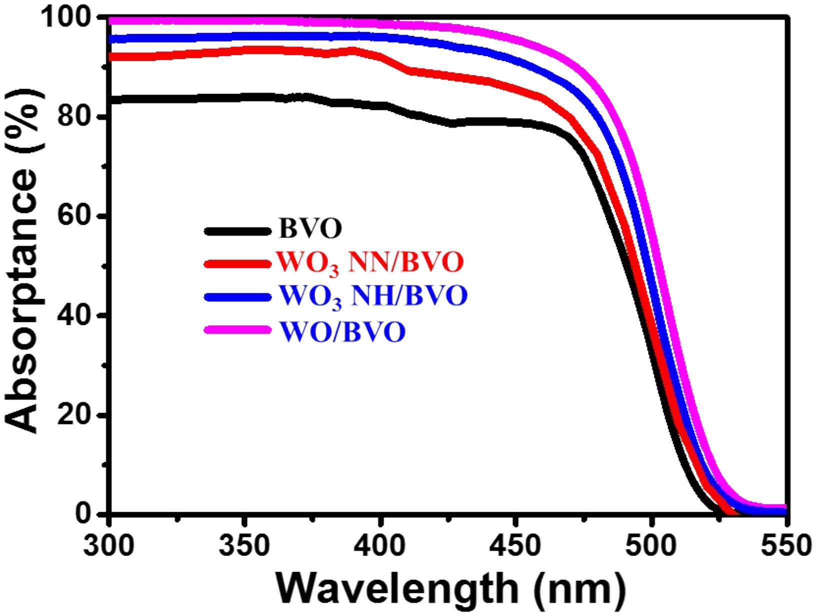

Figure S12. The light absorption spectra of Mo:$BiVO_4$ (BVO) and different conditioned heterojunctions: WO_3 NN/Mo:$BiVO_4$ (WO_3 NN/BVO), WO_3 NH/Mo:$BiVO_4$ (WO_3 NH/BVO) and WO_3(NN/NH)/Mo:$BiVO_4$ (WO/BVO). It can be seen with the help of the WO_3 scaffold, the absorption intensities of the heterojunctions gets enhanced compared to the pure BVO.

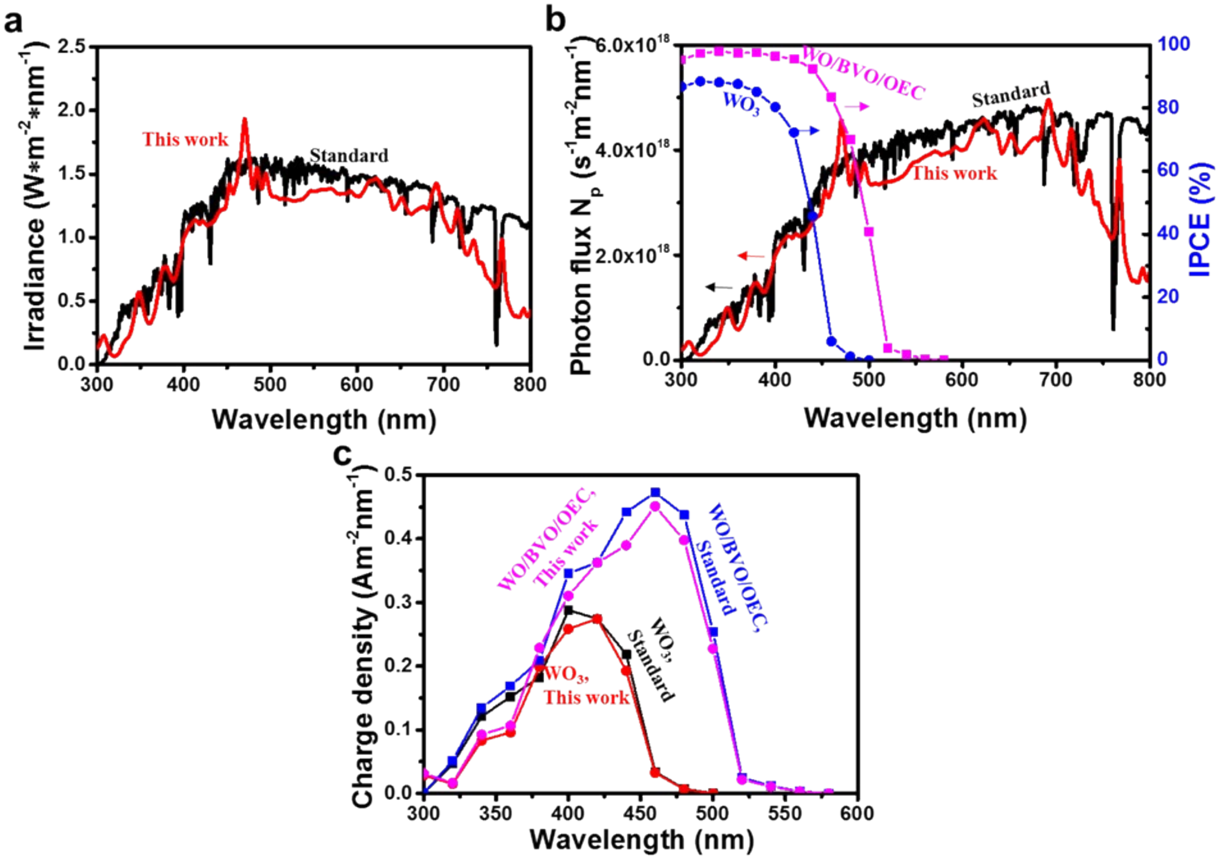

Figure S13. (a) The spectral irradiance of the solar simulator (red curve) and the standard AM 1.5G spectral irradiance (the black curve). (b) Two irradiance curves are converted to the photon numbers in red and black curves. (c) Based on the IPCE measured at 1.23V *vs.* RHE for WO_3 NN/NH in (b), the integration of the current density of WO_3 NN/NH for both standard AM 1.5G and the solar simulator spectrum used in this work lead to 2.7mA/cm^2 and 2.4mA/cm^2 current densities. Similarly the IPCE for the fabricated WO_3(NN/NH)/Mo:$BiVO_4$/Fe-NiOOH (WO/BVO/OEC) at 0.8V vs. RHE upon the standard AM 1.5G spectral irradiance and solar simulator spectrum lead to the integrated results 6.0 and 5.4 mA/cm^2, respectively.

Supplementary References

1. P. M. Rao and X. Zheng, *Proceedings of the Combustion Institute*, 2011, **33**, 1891-1898.
2. P. M. Rao, I. S. Cho and X. Zheng, *Proceedings of the Combustion Institute*, 2013, **34**, 2187-2195.
3. P. M. Rao, L. Cai, C. Liu, I. S. Cho, C. H. Lee, J. M. Weisse, P. Yang and X. Zheng, *Nano Lett.*, 2014, **14**, 1099-1105.